# Accelerated Plate Tectonics

Abstract. *The concept of a stressed elastic lithospheric plate riding on a viscous asthenosphere is used to calculate the recurrence interval of great earthquakes at convergent plate boundaries, the separation of decoupling and lithospheric earthquakes, and the migration pattern of large earthquakes along an arc. It is proposed that plate motions accelerate after great decoupling earthquakes and that most of the observed plate motions occur during short periods of time, separated by periods of relative quiescence.*

From the magnetic record sea floor spreading appears to be uniform over periods of many millions of years. However, from seismic data we know that motions at plate boundaries are not continuous, but occur mainly in jerks separated by tens to hundreds of years. It also appears that major earthquakes are not random in time and location but have some relation to each other. Mogi (*1*), in particular, has investigated the time-space sequence of global seismic activity and has proposed several migration patterns. For example, active seismic areas migrated systematically from Japan to Alaska in the last 35 years, during which this seismic belt was almost completely covered by aftershock areas of great earthquakes. Another pattern started in Central America and migrated to southern Chile in the same period of time. Migration velocities in these belts are 150 to 270 km/year. A particularly clear example of earthquake migration occurred on the Anatolian fault in Turkey after the great earthquake of 1939. The average migration rate, 50 to 100 km/year, has decreased with time. It has been suggested (*2*) that variations in the rotation rate of the earth and great decoupling earthquakes may be related to the start of a migration pattern.

In this report I quantify some of the implications of a simple model of an elastic plate riding on a viscous foundation. This model can be used to estimate the recurrence interval of large earthquakes, the time interval between large earthquakes along an arc, and the distance between decoupling and lithospheric (*3*) earthquakes. The model shows that relative plate rates can be calculated from seismicity only if long enough periods of time are considered.

The recurrence rate of large earthquakes at a particular locale is highly variable. However, the integrated effect of stress release along an arc should show some regularity if plate motions, or strain buildups, are more or less uniform. I propose that patterns of earthquake migration, at least along a particular arc or fault, are due to stress diffusion. Recurrence rates can be estimated from a simple elastic model involving the loading of a plate.

Kanamori (*3*) introduced the concepts of decoupling and lithospheric earthquakes. The first are trench earthquakes in which the boundary between the underthrusting plate and the adjacent restraining plate is broken, temporarily decoupling the two converging lithospheres. A lithospheric earthquake is one that breaks the entire oceanic lithosphere, seaward of the trench. What are the consequences of a great decoupling earthquake? First, one would expect accelerated plate motions in the vicinity of the break. Such motions, in fact, are observed after large interplate earthquakes and seem to have time constants of the order of 5 years (*4*). Post-earthquake motions of several meters per year have been inferred for several large earthquakes (*4, 5*). The rate of underthrusting, or gravitational sinking of the downgoing slab, and the rate of approach of the oceanic lithosphere can be expected to increase when the frictional contact between the oceanic and continental lithospheres is reduced. Continental rebound (sinking) and reduction of the oceanic lithospheric bulge (*6*), previously supported by the relieved stresses, will also occur. The second consequence is that the stress discontinuity resulting from the earthquake will diffuse away from the fault plane and trigger activity along adjacent parts of the arc. In a purely elastic situation this information will flow at elastic wave speeds, and adjacent segments of the arc will know within seconds or minutes that they must support more of the stress imposed by the approaching lithosphere; the immediate aftershocks are presumably triggered by this mechanism. In an elastic layer over a viscous asthenosphere part of the information travels more slowly and damps rapidly. Adjacent segments of the arc will be stressed at a more rapid rate than before the decoupling earthquake, because of both accelerated oceanic plate motions in the vicinity of the decoupling earthquake and the stress wave diffusion from the earthquake. The critical distance, $\lambda_{cr}$, from the boundary between the plates (the location of the decoupling earthquake) and the point of maximum bending moment, presumably the location of a lithospheric earthquake (*3*), is

$$\lambda_{cr} = (\pi/4)[3K(1 - \sigma^2)/Eh_1^3]^{1/4}$$

where $K$ is the buoyancy modulus (product of the density, $\rho$, and the acceleration of gravity, $g$), $\sigma$ is Poisson's ratio, $E$ is the elastic modulus, and $h_1$ is the thickness of the lithosphere. For $h_1 = 50$ km, $E = 10^{12}$ dyne/cm$^2$, and $\sigma = 0.25$, $\lambda_{cr}$ is 90 km. This is about the separation between the 1896 decoupling earthquake and the 1933 lithosphere earthquake of Sanriku (*3*).

In the period between large earth-

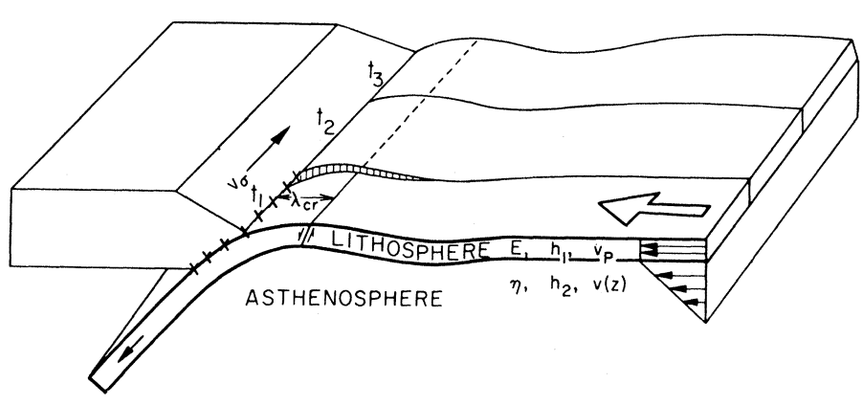


Fig. 1. The model. The oceanic lithosphere, of thickness $h_1$ and modulus $E$ under stress $\sigma_x$, is assumed to be sliding on an asthenosphere of viscosity $\eta$ and thickness $h_2$. The flow patterns are indicated schematically by the arrows to the right. A decoupling earthquake is indicated by the crosses, and $\lambda_{cr}$ is the distance between the decoupling earthquake and the point of maximum tension. The decoupling earthquake occurs at time $t_1$, decreasing stresses in the lithosphere closest to the viewer and increasing stresses at the adjacent segments of the arc boundary, leading to subsequent earthquakes at times $t_2$ and $t_3$. The velocity of propagation of the stress wave is denoted $v_\sigma$.

quakes along island arcs the oceanic lithosphere is compressed by the more or less steady plate tectonic driving forces. This compression is most severe near the trench but may extend well into the oceanic lithospheric plate. When the stress near the boundary reaches a critical level, underthrusting will occure along a segment of the arc. Alternatively, a tensional earthquake may occur in the lithospheric bulge (see Fig. 1). The sudden stress release generates a kinematic stress wave (*7*) which serves to increase the stress along the arc boundary and to decrease the stress in the plate interiors. Table 1 gives values of the velocity of this wave as a function of time for a viscosity of $5 \times 10^{19}$ poise, the value found to be appropriate for the arc boundary in Japan from measurements of postseismic slip (*4*).

Most of the plate boundary in the Alaska-Aleutians area appears to have been broken between 1899 and 1905. In this period there were ten events of magnitude greater than 7.8 distributed along the arc. The few gaps in this period were filled by events in 1878, 1880, 1906, 1909, and 1912. This boundary broke again between 1957 and 1965, in which period there were five events of magnitudes greater than 7.9. With the exception of the 1899 site, most gaps in the latest pattern were probably filled by events in 1927, 1938, and 1949. The area near Sitka, the most recent gap, ruptured in 1972, 1927, and 1880. Considering the arc as a whole, the repeat time is 60 years. A breaking cycle seems to involve about 6 to 8 years of intensive activity and 30 to 40 years for completion. The implied rates of stress propagation are of the order of 60 to 125 km/year, taking the distance between centers of adjacent aftershock zones. Rates will actually be somewhat less than this when the zone of breakage of large earthquakes and their aftershocks is taken into account.

Consider the recurrence interval between large events along a stretch of the boundary of the Pacific plate such as the Alaska-Aleutian arc. In this region relative plate motions are of the order of 7 cm/year (*8*). The 1964 Alaskan event gave a coseismic strain drop of about $4 \times 10^{-5}$ (*9*). Assuming that strains are accumulated over the characteristic length of a 50-km-thick plate, $\sim 100$ km, this strain will be built up in

$$t = \frac{(4 \times 10^{-5})(10^7 \text{ cm})}{(7 \text{ cm/year})} = 57 \text{ years}$$

Table 1. Parameters of stress diffusion.

| $t$ (year) | $x$ (km) | $v$ (km/year) |
|---|---|---|
| 1 | 170 | 170 |
| 5 | 390 | 78 |
| 10 | 520 | 52 |
| 20 | 775 | 39 |

which is in agreement with the recurrence interval between arc-breaking events in the Alaska-Aleutian region. Since the recurrence time depends on both convergence rates and lithospheric thickness, regions of continental collision, such as the Himalayas, might be expected to have larger recurrence intervals. This seems to be the case in India and central Asia.

The time interval between decoupling and lithospheric earthquakes in the same plate is a function of loading rates rather than diffusion rates. Assume that coseismic and postseismic slip resulted in a strain release of $0.3 \times 10^{-4}$ (3 m of slip over a characteristic length of 100 km) for the 1896 Sanriku decoupling event and that the boundary was healed in about 5 years, the "time constant" for accelerated plate motions in Japan. Then this strain was again achieved in 33 years at plate rates of 9 cm/year. Conditions should then have been appropriate for another major failure in the Sanriku region at about the time of the 1933 Sanriku lithospheric earthquake. Previous earthquakes offshore of Sanriku, accompanied by tsunamis, occurred in 1861, 1835, and 1793, giving an average repeat time of 35 years. Another event, of magnitude 7.9, occurred in the Sanriku area in 1968, 35 years after the 1933 event.

The mechanical picture I adopt for delayed effects (see Fig. 1) is similar to the lithospheric stress guide hypothesis of Elsasser (*10*). The lithosphere, of thickness $h_1$, is assumed to slide on a viscous asthenosphere, of thickness $h_2$ and viscosity $\eta$, in response to a horizontal stress, $\sigma_x$. The velocity of steady sliding, $v_p$, is

$$v_p = \frac{\sigma_x}{\eta} \frac{h_1 h_2}{L}$$

where $L$ is the unconstrained length of the sliding lithosphere. The plate is under stress ($\sigma_x$), but is relatively stationary at a trench boundary until the frictional stress between the oceanic and continental plates is exceeded, at which time failure and slippage occur. A decoupling earthquake (*3*) results in a stress drop at the boundary which diffuses in all directions, in particular along the plate boundary. While the plates are decoupled, accelerated relative motion between the two plates occurs.

Taking $h_1 = 50$ km, $h_2 = 200$ km, $L = 1000$ km, $\eta = 5 \times 10^{19}$ poise, and $\sigma_x = 100$ bars, we obtain 30 cm/year, a reasonable rate for unconstrained motions. However, this is the steady state or terminal velocity of the plate. The information that stress has been released at the boundary of the plate will take about 30 years to affect the whole of a 1000-km-long plate. Immediately after a decoupling earthquake the effective plate length is likely to be close to the characteristic wavelength of a 50-km plate, or about 100 km. In this case the plate motion near the boundary will be about 3 m/year until the boundary heals. Postseismic slip of several meters per year has been inferred for the 1946 Nankaido earthquake (*5*), this rate decreasing rapidly for the several years following the earthquake.

The displacement, $u$, of a point on the plate satisfies the diffusion equation (*7, 10*)

$$\frac{\partial u}{\partial t} = k \frac{\partial^2 u}{\partial x^2}; \; k = h_1 h_2 E/\eta$$

The mean distance $x$ which a disturbance propagates in time $t$ is approximately

$$x = (4kt)^{1/2}$$

Taking $h_1$, $h_2$, $\eta$, and $E$ as before, we obtain the values in Table 1.

With these parameters the stress diffusion rate is 170 km/year for the first year, decreasing to 50 km/year after 10 years. The distance reached by the stress wave after 10 years is 520 km. Considering the simplicity of the model and the uncertainties of the parameters, the agreement with the time intervals between adjacent events along an arc and migration rates (*1*) is remarkably good.

The sinkage rate of the portion of slab broken off by a decoupling earthquake, approximated as a sphere of radius $a$ sinking through a viscous half-space, is

$$v = \frac{2}{9} \Delta\rho g a^2/\eta$$

where $v$ is the terminal velocity and $\Delta\rho$ is the density contrast. Taking $a$ as 60 km, $\eta$ as $5 \times 10^{19}$ poise, and $\Delta\rho$ as 0.05 g/cm$^3$, we obtain 3 m/year for the terminal sinking velocity.

The simple model of a stressed elastic

lithosphere explains the recurrence interval of arc-breaking events and the separation of decoupling and lithospheric earthquakes. The viscosity found from postseismic rebound (*4*) for an arc event gives reasonable migration velocities for great earthquakes along major fault systems. Meters per year of displacement for lithospheric convergence and sinkage are appropriate after a major decoupling earthquake. Such rates with time constants of the order of 5 years reopen the question of excitation of the Chandler wobble and changes in the length of day (*2*).

DON L. ANDERSON
*Seismological Laboratory, California Institute of Technology, Pasadena 91125*

**References and Notes**

1. K. Mogi, *J. Phys. Earth* **16**, 30 (1968); *Bull. Earthquake Res. Inst. Tokyo Univ.* **46**, 53 (1968).
2. D. L. Anderson, *Science* **186**, 49 (1974).
3. H. Kanamori, *Tectonophysics* **12**, 187 (1971).
4. A. Nur and G. Mavko, *Science* **183**, 204 (1974).
5. T. J. Fitch and C. H. Scholz, *J. Geophys. Res.* **76**, 7260 (1971).
6. T. C. Hanks, *Geophys. J. R. Astron. Soc.* **23**, 173 (1971).
7. M. H. P. Bott and D. S. Dean, *Nature (Lond.)* **243**, 339 (1973).
8. J. B. Minster, T. H. Jordan, P. Molnar, E. Haines, *Geophys. J. R. Astron. Soc.* **36**, 541 (1974).
9. H. Kanamori, *J. Geophys. Res.* **75**, 5029 (1970).
10. W. H. Elsasser, *ibid.* **74**, 4744 (1971).
11. Contribution No. 2549, Division of Geological and Planetary Sciences, California Institute of Technology. Supported by a Chevron Oil Company research grant and by contract 14-08-0001-1412 with the U.S. Geological Survey.

23 October 1974; revised 8 January 1975

## Partial Amino Acid Sequence of Rabbit $\beta_2$-Microglobulin

Abstract. *The amino acid sequence of the first 35 residues of a low-molecular-weight protein obtained from the urine of rabbits treated with sodium dichromate was determined and shown to be identical with human $\beta_2$-microglobulin in 30 positions. Rabbit $\beta_2$-microglobulin, like the human protein, is strikingly homologous to the constant regions of rabbit immunoglobulin G, particularly the $C_H3$ region.*

$\beta_2$-Microglobulin is a low-molecular-weight protein found in normal biological fluids (*1*) and on the surfaces of a variety of different cell types (*2*). The complete amino acid sequence of human $\beta_2$-microglobulin (*3*) shows that it is strikingly homologous to immunoglobulin G (IgG) and in many ways resembles the individual domains of the constant region of the light and heavy chains (*4*). Recent data (*5*) indicate that $\beta_2$-microglobulin is closely associated with the histocompatibility antigens on cell surfaces and that it may represent the light chain of the human histocompatibility (HL-A) antigens. The similarity of $\beta_2$-microglobulin to IgG and its close association with the HL-A antigens has a number of important implications for the evolution of the immune and histocompatibility systems and for the structure of the HL-A antigens (*6, 7*). As a result, numerous attempts have been made to obtain similar proteins from other species for evolutionary comparisons and for functional studies.

A protein that resembles $\beta_2$-microglobulin in molecular weight, charge, and amino acid composition has been purified from the urine of rabbits treated with sodium chromate (*8*). We report here the partial amino acid sequence of this protein and show that it is very similar to both $\beta_2$-microglobulin and a homolog of $\beta_2$-microglobulin obtained from dogs (*9*). Like the human protein, rabbit $\beta_2$-microglobulin is homologous to the constant region of the heavy chain ($C_H$) of IgG.

The rabbit protein was prepared as described (*8*). Half-cystines were reduced in the presence of 6*M* guanidine hydrochloride and alkylated with iodoacetamide or [$^{14}$C]iodoacetamide (*10*). Excess reagents were removed by gel filtration on Sephadex G-25 in 5 percent formic acid. Manual sequence determinations on the intact protein (100 to 200 nmole) and on isolated peptides were carried out by the dansyl-Edman technique (*11*). Automatic sequence analysis of the reduced and alkylated protein (130 to 170 nmole) was performed in a Beckman model 890 C automatic sequencer and with the use of the Quadrol double cleavage program (Beckman Instruments).

Phenylthiohydantoins were identified quantitatively by gas chromatography on columns of Chromasorb SP400 in a Beckman GC-65 gas chromatograph. Qualitative identification of the phenylthiohydantoins was made by thin-layer chromatography on Chromagram silica gel sheets with fluorescent indicator (Eastman Kodak) with the use of solvent systems V and IV of Jeppson and Sjöquist (*12*) and by thin-layer chromatography on polyamide layers (*13*). The presence of half-cystine was determined by dissolving all samples from the sequencer in Aquasol and counting for $^{14}$C in a Packard Tri-Carb 3003 scintillation counter. The presence of arginine (*14*) or histidine was determined colorimetrically.

Tryptic peptides were obtained from digests of 4 to 5 mg of the reduced and alkylated protein. Peptide TN1 ($Arg_{1.1}$ $Glu_{1.0}$ $Val_{0.9}$) (*15*) was purified initially by gel filtration of a tryptic digest on Sephadex G-25 in 0.015*M* $NH_4OH$ which was 10 percent in 1-propanol. Extraction of the lyophilized fraction containing the material of lowest molecular weight with pyridine-acetate, *p*H 6.5 (*16*), gave peptide TN1 as a precipitate in 25 percent yield. Peptide TN2a ($Asp_{1.1}$ $Glu_{1.2}$ $Pro_{0.9}$ $Ala_{1.0}$ $Val_{0.9}$ $Tyr_{0.5}$) was obtained in 24 percent yield from a digest of the protein by high-voltage paper electrophoresis at *p*H 4.7 followed by electrophoresis at *p*H 1.9 (*17*).

The amino acid sequence of the first 35 residues of the rabbit protein is shown in Fig. 1, which also summarizes the methods used to identify each residue. The yield at each step was established from the gas chromatographic analysis. Yields were 77 percent for $Val^1$, 44 percent for $Ala^4$, 18 percent for $Ser^{11}$ and 1 percent for $Gly^{18}$. Up to step 18 no contamination from previous steps or phase changes were apparent. After step 18 yields were decreased and the identification of the phenylthiohydantoins from residues 19 to 35 depended primarily upon qualitative techniques. Half-cystinyl residue 25 was determined in about 3 percent yield by counting the [$^{14}$C]carboxamidomethyl derivative. The sequence of residues 1 to 10 was confirmed by dansyl-Edman analysis of the intact protein and of peptides TN1 and TN2a. Peptide TN2a probably arose as the result of chymotryptic activity in the trypsin preparation. The human protein is also highly susceptible to chymotryptic cleavage at $Tyr^{10}$ (*3*).

In Figure 1 are shown the positions where the rabbit homolog differs from human $\beta_2$-microglobulin (*3*) and from the dog homolog (*9*). Of the 35 residues compared, there are only 5 differences from the human protein, which has residues $Ile^1$, $Thr^4$, $Lys^6$, $Ile^7$, and $Ser^{20}$ rather than those shown for the rabbit homolog. The dog homolog has $Lys^6$ and $Ile^7$ in common with the human protein and differs from the rabbit